

Tunneling Measurements in Twisted Bilayer Graphene



S Ramachandra Bangari

Undergraduate

Department Of Instrumentation and Applied Physics
Indian Institute of Science

Submitted in partial satisfaction of the requirements for the
Degree of Bachelor of Science (Research)
in Physics

Supervisor Dr. Chandni U

May 2021

Declaration

I certify that -

- (a) The work contained in this report has been done by me under the guidance of my supervisor.
- (b) The work has not been submitted to any other Institute for any degree or diploma.
- (c) I have conformed to the norms and guidelines given in the Ethical Code of Conduct of the Institute.
- (d) Whenever I have used materials (data, theoretical analysis, figures, and text) from other sources, I have given due credit to them by citing them in the text of the thesis and giving their details in the references.

Date - 21 May, 2021

S Ramachandra Bangari

Place - IISc, Bangalore

11-01-00-10-91-16-1-14477

UG PROGRAMME
INDIAN INSTITUTE OF SCIENCE
BANGALORE - 560012, INDIA



CERTIFICATE

This is to certify that the Bachelor's thesis entitled "**Tunneling Measurements in Twisted Bilayer Graphene**" submitted by **S Ramachandra Bangari** (Sr No. 11-01-00-10-91-16-1-14477) to Indian Institute of Science, Bangalore towards partial fulfilment of requirements for the award of degree of Bachelor of Science (Research) in Physics is a record of bona fide work carried out by him under my supervision and guidance during Academic Year, 2020-21.

Date - 21 May, 2021

Dr. Chandni U

Place - IISc, Bangalore

Dept. of Instrumentation and Applied Physics

Indian Institute of Science
Bangalore - 560012, India

Abstract

...

Acknowledgements

vvnmjv

Contents

1	Introduction	1
1.1	Aim of the thesis	1
1.2	Motivation	1
2	Theory	2
2.1	Graphene	2
2.2	Bilayer Graphene	5
2.3	Twisted Bilayer Graphene	7
2.3.1	Moire Superlattices	7
2.3.2	Continuum Model	8
2.3.3	Flat bands in twBLG	14
2.3.4	Experimental Signatures of twBLG	15
3	Methods	17
3.1	Exfoliation of Graphene and hBN	17
3.2	Flake selection	19
3.3	Stamp creation	19
3.4	Pickup and Transfer Process	20
3.5	Twisted Bilayer Graphene Fabrication	23
4	Measurements	25
5	Conclusions	26
5.1	Discussion	26
5.2	Future Work	26

List of Figures

2.1	Graphene Lattice and its Brillouin zone. Left: Two interpenetrating triangular lattices forming graphene honeycomb lattice. a_1 and a_2 are lattice vectors and $\delta_i, i = 1, 2, 3$ are the nearest neighbour vectors. Right: Corresponding Brillouin zone that shows high symmetry points. The Dirac cones are located at K and K' points. Figure adapted from [Geim]	2
2.2	Electronic dispersion of graphene. Left: Energy spectrum of the honeycomb lattice in units of t for non zero t and t' . Here $t = 2.7eV$ and $t' = -0.2t$. Right: Zoom in of the energy bands near one of the Dirac points. Figure adapted from [Geim]	4
2.3	Bernal stack bilayer graphene lattice with hopping terms and its Brillouin zone. Left: Two monolayer graphene in AB stacking forming bernal stack bilayer graphene lattice. $\gamma_0, \gamma_1, \gamma_3$ and γ_4 are the hopping terms. Right: Corresponding Brillouin zone that shows high symmetry points. Figure adapted from [Geim]	5
2.4	Electronic dispersion of bilayer graphene when $\Delta = 0$ (left) and $\Delta \neq 0$ (right). A band gap Δ_g opens up in the presence of an external displacement field. Figure adapted from [Zhang2009]	7
2.5	twBLG moire pattern and its mini Brillouin zone. Left: The moiré pattern as seen in twBLG. The moiré wavelength is $\lambda = \frac{a}{2\sin(\theta/2)}$. Right: The mini Brillouin zone is constructed from the difference between the two $K(K')$ wavevectors for the two layers. K_s, K'_s, M_s and Γ_s denote points in the mini Brillouin zone. Figure adapted from [Cao2018]	8
2.6	Cont. Figure adapted from [Bistritzer12233]	9
2.7	Cont. Figure adapted from [Bistritzer12233]	12
2.8	Cont. Figure adapted from [Bistritzer12233]	13
2.9	Electronic band structure of twBLG	15

2.10 twBLG transport signatures. Top: Four-terminal longitudinal resistance plotted against carrier density at different perpendicular magnetic fields from 0 T (black trace) to 480 mT (red trace). Bottom: Colour plot of longitudinal resistance against carrier density and temperature, showing different phases including metal, band insulator (BI), correlated state (CS) and superconducting state (SC). Figure adapted from [Lu2019] .	16
3.1 Pickup and Transfer of thin hBN on gold pad	23

Chapter 1

Introduction

1.1 Aim of the thesis

1.2 Motivation

Chapter 2

Theory

2.1 Graphene

Graphene is a monolayer of carbon atoms arranged in a honeycomb lattice, that can be thought of as two interpenetrating triangular sublattices, with two nonequivalent carbon atoms.

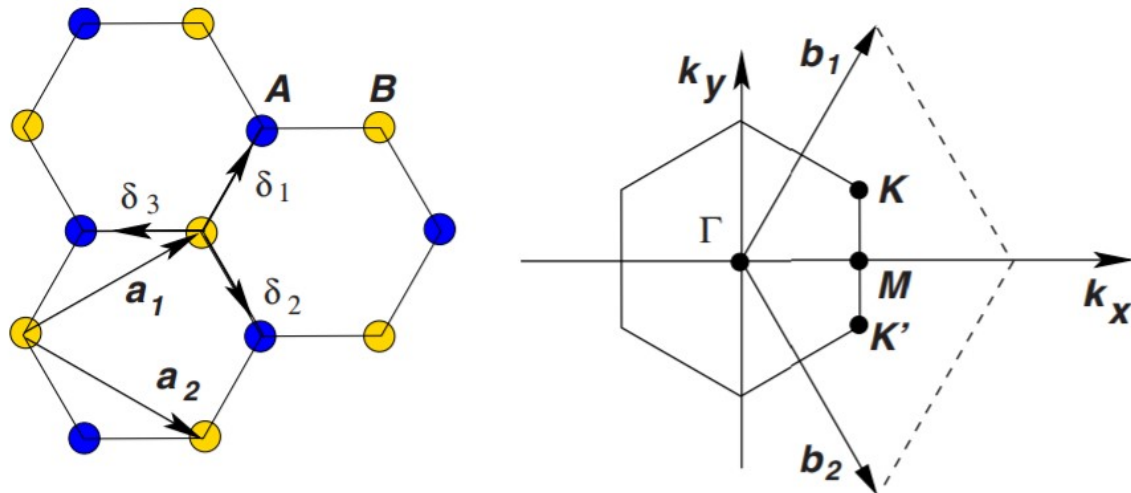


Figure 2.1: Graphene Lattice and its Brillouin zone. Left: Two interpenetrating triangular lattices forming graphene honeycomb lattice. a_1 and a_2 are lattice vectors and $\delta_i, i = 1, 2, 3$ are the nearest neighbour vectors. Right: Corresponding Brillouin zone that shows high symmetry points. The Dirac cones are located at K and K' points. Figure adapted from [Geim]

The primitive lattice vectors for the lattice are given by (see fig. 2.1):

$$a_1 = \frac{a}{2}(3, \sqrt{3}), a_2 = \frac{a}{2}(3, -\sqrt{3}) \quad (2.1)$$

The reciprocal lattice vectors are given by (see fig. 2.1):

$$b_1 = \frac{2\pi}{3a}(1, \sqrt{3}), b_2 = \frac{2\pi}{3a}(1, -\sqrt{3}) \quad (2.2)$$

The wave vectors of the high symmetry points in the first Brillouin zone are given below, where K and K' are two nonequivalent corners known as the Dirac points, as shown in fig. 2.1.

$$\Gamma = (0, 0), K = \frac{2\pi}{3a}(1, \frac{1}{\sqrt{3}}), K' = \frac{2\pi}{3a}(1, -\frac{1}{\sqrt{3}}), M = \frac{2\pi}{3a}(1, 0) \quad (2.3)$$

The electronic structure of graphene can be derived using the tight binding model, considering nearest and next nearest neighbour hopping. The Hamiltonian becomes:

$$H = -t \sum_{<ij>, \sigma} (a_{\sigma,i}^\dagger b_{\sigma,j} + H.c) - t' (a_{\sigma,i}^\dagger a_{\sigma,j} + b_{\sigma,i}^\dagger b_{\sigma,j} + H.c.) \quad (2.4)$$

where $a_{\sigma,i}$, $a_{\sigma,i}^\dagger$ and $b_{\sigma,i}$, $b_{\sigma,i}^\dagger$ are the annihilation and creation operators on site A and B, with spin σ , respectively. t is the nearest neighbour hopping energy $\approx 2.7\text{eV}$ and t' is the next nearest neighbour hopping energy $\approx -0.2t$. We can diagonalise the Hamiltonian and derive the electronic dispersion to be [Geim]:

$$E_\pm(\mathbf{k}) = \pm t\sqrt{f(\mathbf{k}) + 3} - t'f(\mathbf{k}), f(\mathbf{k}) = \cos(\frac{\sqrt{3}}{2}k_y a)\cos(\frac{3}{2}k_x a) + 2\cos(\sqrt{3}k_y a) \quad (2.5)$$

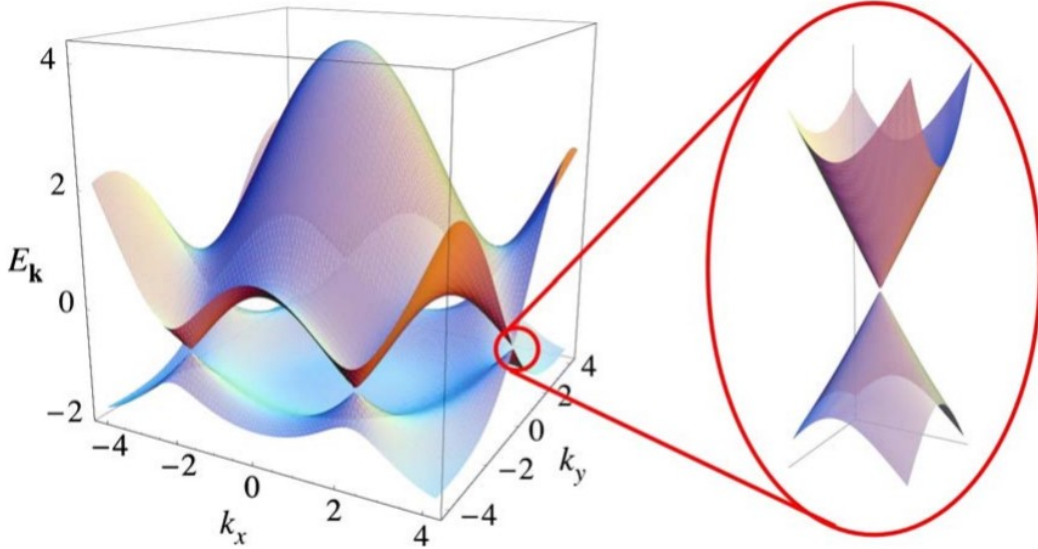


Figure 2.2: Electronic dispersion of graphene. Left: Energy spectrum of the honeycomb lattice in units of t for non zero t and t' . Here $t = 2.7\text{eV}$ and $t' = -0.2t$. Right: Zoom in of the energy bands near one of the Dirac points. Figure adapted from [Geim]

This gives symmetric band structure for holes and electrons around zero energy, if we take t' to be zero. But the electron-hole symmetry is broken and the upper and lower bands become asymmetric for finite next nearest neighbour hopping. In fig. 2.2, the full band structure of graphene is shown. A zoom in of the band structure close to one of the Dirac points is also shown. This dispersion can be obtained by expanding the full band structure, close to \mathbf{K} or \mathbf{K}' vector, i.e., $\mathbf{k} = \mathbf{K} + \mathbf{q}$ ($|\mathbf{q}| \ll |\mathbf{K}|$):

$$E_{\pm}(\mathbf{q}) = \pm v_F |\mathbf{q}| + O[(q/K)^2] \quad (2.6)$$

where \mathbf{q} is the momentum measured relatively to the Dirac points and v_F is the Fermi velocity, given by $v_F = 3ta/2$.

The above equation shows that the energy bands linearly cross at the Dirac points and hence the graphene acts as a zero band gap material with a linear dispersion. The approximation is valid for small carrier densities. From equation (2.6), the Hamiltonian near the Dirac points can be written as:

$$H_{Dirac} = \begin{bmatrix} 0 & q_x - iq_y \\ q_x + iq_y & 0 \end{bmatrix} = v_F \sigma \cdot \mathbf{q} \quad (2.7)$$

where σ is the corresponding Pauli matrices. This is equivalent to the equation for massless chiral Dirac fermions in 2D where the speed of light has been replaced by v_F and with a pseudospin spinor structure related to the graphene sublattices. Many of the interesting properties of graphene can be explained using this unique and interesting dispersion.

2.2 Bilayer Graphene

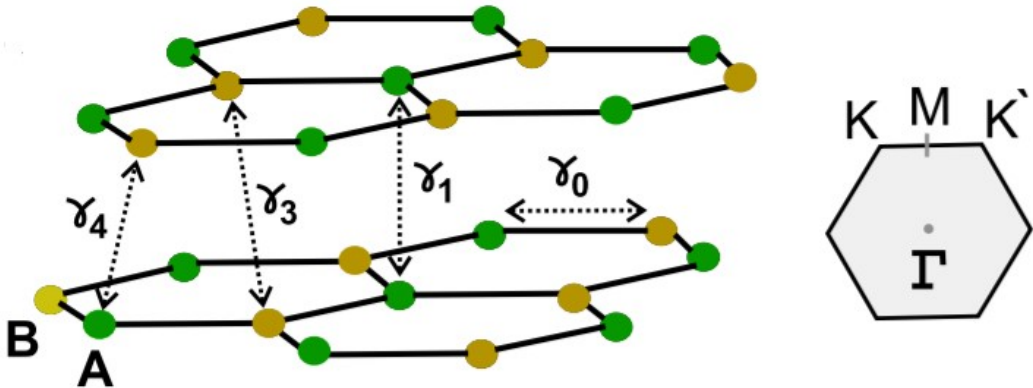


Figure 2.3: Bernal stack bilayer graphene lattice with hopping terms and its Brillouin zone. Left: Two monolayer graphene in AB stacking forming bernal stack bilayer graphene lattice. γ_0 , γ_1 , γ_3 and γ_4 are the hopping terms. Right: Corresponding Brillouin zone that shows high symmetry points. Figure adapted from [Geim]

Bilayer graphene usually refers to AB stacking or Bernal stacking in which two layers of graphene are stacked on top of each other such that the two layers are shifted by one atomic spacing, as shown in fig. 2.3. The tight binding model gives us the energy dispersion of bilayer graphene. Considering various hopping terms - in-plane nearest neighbour hopping, $\gamma_0 \approx 2.7eV$, hopping between atom A_1 and atom A_2 , $\gamma_1 \approx 0.4$, hopping between atom B_1 and atom B_2 , $\gamma_1 \approx 0.3$ and hopping between atom $A_1(A_2)$ and atom $B_2(B_1)$, the tight-binding Hamiltonian becomes:

$$H = -\gamma_0 \sum_{\langle i,j \rangle, m, \sigma} (a_{i,m,\sigma}^\dagger b_{j,m,\sigma} + H.c.) - \gamma_1 \sum_{j,\sigma} (a_{j,1,\sigma}^\dagger a_{j,2,\sigma} + H.c.) \\ - \gamma_3 \sum_{j,\sigma} (b_{j,1,\sigma}^\dagger b_{j,2,\sigma} + H.c.) - \gamma_4 \sum_{j,\sigma} (a_{j,1,\sigma}^\dagger b_{j,2,\sigma} + a_{j,2,\sigma}^\dagger b_{j,1,\sigma} + H.c.) \quad (2.8)$$

where $a_{i,m,\sigma}(b_{j,m,\sigma})$ annihilates an electron on sublattice $A(B)$ with spin σ on plane $m = 1, 2$. If we apply a perpendicular electric field to the system, an electrochemical potential Δ is added between the layers. The Hamiltonian in the k space near the $K(K')$ points, ignoring the weaker hopping terms γ_3 and γ_4 , can be represented as [Geim]:

$$H_{K/K'} = \begin{bmatrix} -\frac{\Delta}{2} & v_F k & 0 & 0 \\ v_F k & -\frac{\Delta}{2} & \gamma_1 & 0 \\ 0 & \gamma_1 & \frac{\Delta}{2} & v_F k \\ 0 & 0 & v_F k & \frac{\Delta}{2} \end{bmatrix} \quad (2.9)$$

The resultant electronic dispersion near the Dirac points is given by:

$$E_\pm^2 = \frac{\Delta^2}{4} + v_F^2 k^2 + \frac{\gamma_1^2}{2} \pm \sqrt{\Delta^2 v_F^2 k^2 + \gamma_1^2 v_F^2 k^2 + \frac{\gamma_1^4}{4}} \quad (2.10)$$

This equation gives rise to four solutions, hence, four bands near the $K(K')$ points, as shown in fig. 2.4. For $\Delta = 0$ and $v_F \ll \gamma_1$, the lowest two bands are given by:

$$E \approx \frac{v_F^2 k^2}{\gamma_1} \quad (2.11)$$

We see that even bilayer graphene does not have a band gap when no external displacement field is applied. But unlike monolayer graphene which has a linear dispersion, bilayer graphene has a parabolic dispersion near the Dirac points, with effective mass $m^* = \frac{\gamma_1}{2v_F^2}$. For $\Delta \neq 0$ and $\Delta \ll \gamma_0$, the lowest two bands are given by:

$$E \approx \frac{\Delta}{2} - \frac{\Delta v_F^2 k^2}{\gamma_1} + \frac{v_F^4 k^4}{\gamma_1^2 \Delta} \quad (2.12)$$

In the presence of a displacement field, we see that a band gap opens up, which can be tuned by changing the applied perpendicular electric field.

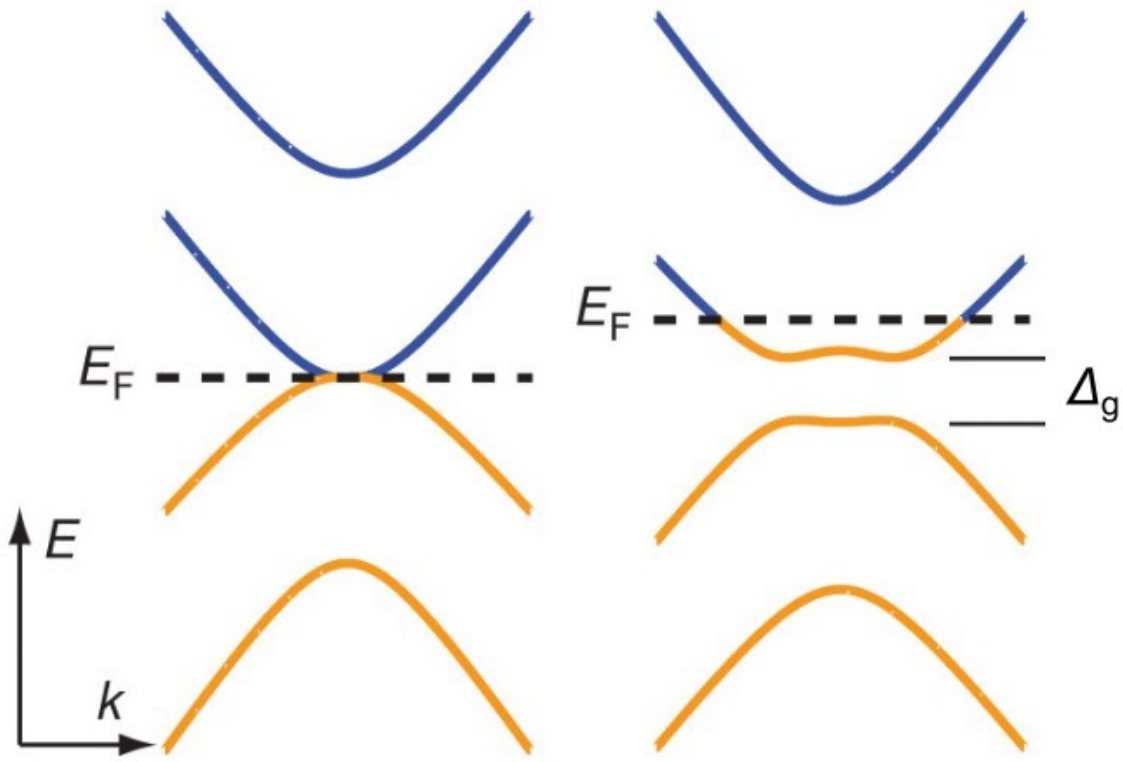


Figure 2.4: Electronic dispersion of bilayer graphene when $\Delta = 0$ (left) and $\Delta \neq 0$ (right). A band gap Δ_g opens up in the presence of an external displacement field. Figure adapted from [Zhang2009]

2.3 Twisted Bilayer Graphene

2.3.1 Moire Superlattices

A geometric interference pattern, known as moire pattern, is formed when two dimensional crystals with a lattice mismatch or a relative twist between them are stacked on top of each other. The wavelength of the moire pattern in case two layers of graphene is given by:

$$\lambda = \frac{(1 + \delta)a}{\sqrt{2(1 + \delta)(1 - \cos\theta) + \delta^2}} \quad (2.13)$$

where a is the lattice constant of graphene, θ is the twist angle between the two layers and δ is the lattice mismatch between the two layers. Moire pattern gives rise to effective superlattice potential with a periodicity different from the original lattice. We can see that the moire wavelength becomes much larger than the lattice constant for small twist angles. When λ becomes comparable to the Fermi wavelength, the electronic structure is significantly modified. For example, aligned graphene-hBN heterostructures give rise to secondary Dirac points as a result of the moire superlattice potential.

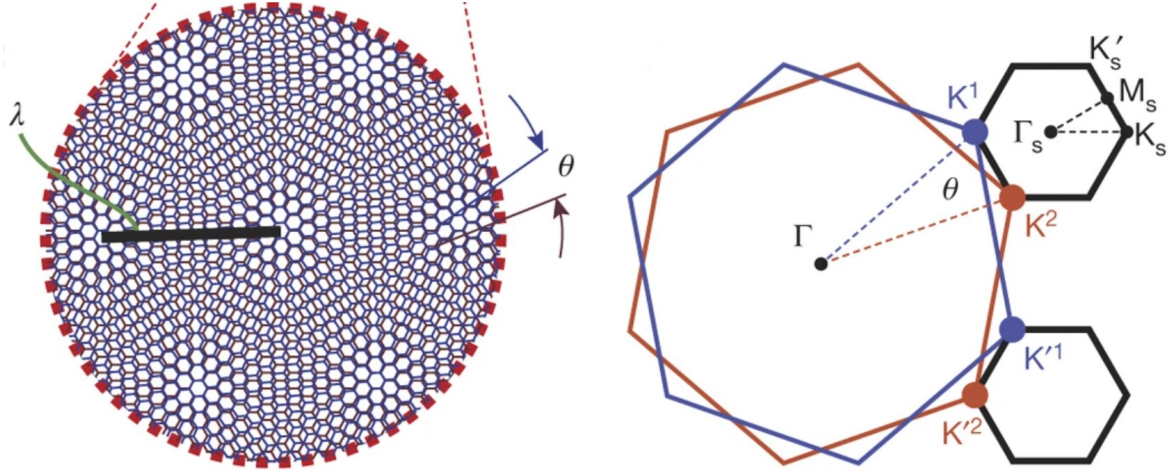


Figure 2.5: twBLG moiré pattern and its mini Brillouin zone. Left: The moiré pattern as seen in twBLG. The moiré wavelength is $\lambda = \frac{a}{2\sin(\theta/2)}$. Right: The mini Brillouin zone is constructed from the difference between the two $K(K')$ wavevectors for the two layers. K_s, K'_s, M_s and Γ_s denote points in the mini Brillouin zone. Figure adapted from [Cao2018]

2.3.2 Continuum Model

The geometry of the bilayer system is characterised by a twist angle θ and a translation vector \mathbf{d} . But commensurability is determined only by the twist angle. In a commensurate structure, sliding one layer with respect to another modifies the unit cell but leaves the bilayer crystalline. So, let's consider AB stacking as the aligned configuration. The positions of the carbon atoms in the two layers are then \mathbf{R} and $\mathbf{R}' = M(\theta)(\mathbf{R} - \tau) + \mathbf{d}$, where τ is a vector connecting the two atoms in the unit cell, and M is a two dimensional rotation matrix within the graphene plane.

The bilayer forms a two-dimensional crystal only at a discrete set of commensurate twist angles. Bloch's theorem doesn't apply microscopically at generic twist

angles and hence direct electronic structure calculations are not possible. For twist angles larger than a few degrees, except for a small set of angles that give low-order commensurate structure, the two layers are electronically isolated. As the twist angle reduces, interlayer coupling strengthens and quasiparticle velocity at Dirac point decreases. We derive a low-energy effective Hamiltonian valid for any value of \mathbf{d} and for small twist angles, $\theta < 10^\circ$ [Bistritzer12233].

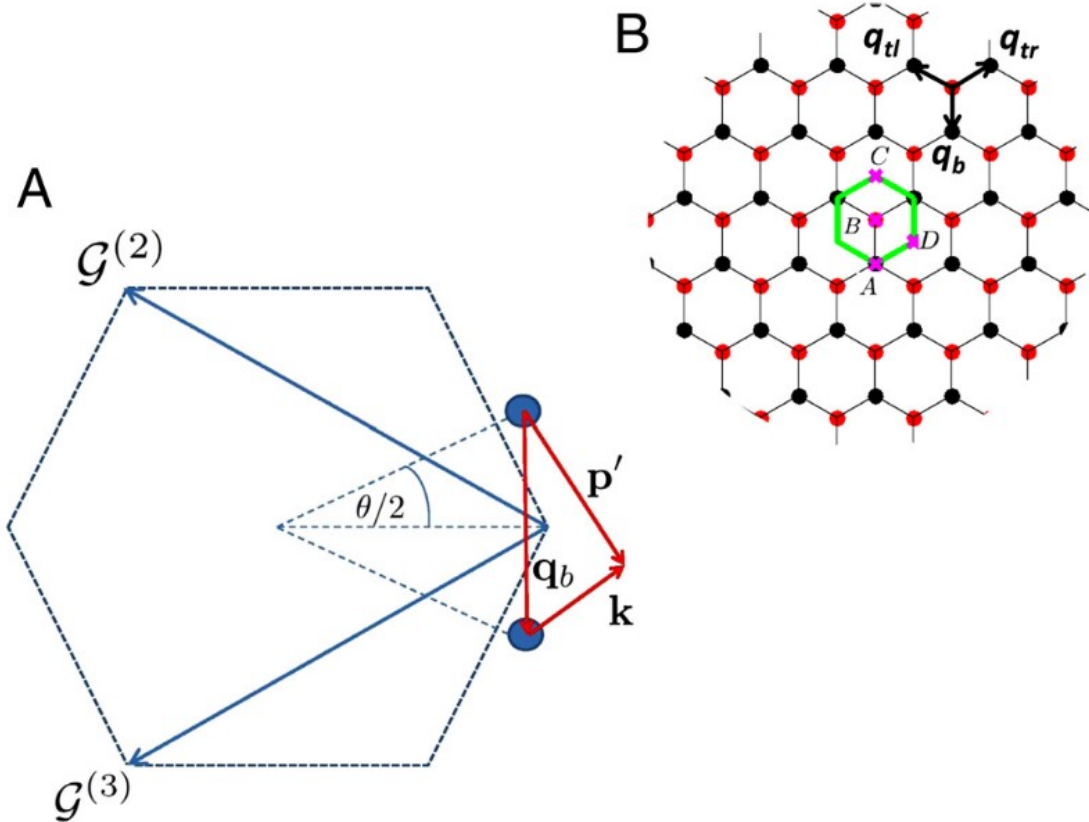


Figure 2.6: Cont. Figure adapted from [Bistritzer12233]

The low-energy continuum model Hamiltonian has three terms: two single-layer Dirac-Hamiltonian terms that are associated with the isolated graphene sheets and a tunneling term that accounts for the hopping between the layers. The Dirac-Hamiltonian for a layer rotated by an angle θ with respect to a fixed coordinate system is given by [Geim]:

$$h_{\mathbf{k}}(\theta) = -vk \begin{bmatrix} 0 & e^{i(\theta_{\mathbf{k}}-\theta)} \\ e^{-i(\theta_{\mathbf{k}}-\theta)} & 0 \end{bmatrix} \quad (2.14)$$

where \mathbf{k} is the momentum measured from the Dirac point, v is the Dirac velocity, $\theta_{\mathbf{k}}$ is the momentum orientation relative to the x axis. Choosing the coordinate system as shown in fig. 2.6, the decoupled bilayer Hamiltonian is $|1\rangle h(\theta/2) \langle 1| + |2\rangle h(-\theta/2) \langle 2|$, where $\langle i|i\rangle$ projects onto layer i .

Assuming that the interlayer tunneling amplitude between the π -orbitals is a smooth function of spatial separation projected onto the graphene planes, we derive a continuum model. The matrix element,

$$T_{\mathbf{k}\mathbf{p}'}^{\alpha\beta} = \langle \Psi_{\mathbf{k}\alpha}^{(1)} | H_T | \Psi_{\mathbf{p}'\beta}^{(2)} \rangle \quad (2.15)$$

of the tunneling Hamiltonian H_T , describes a process in which an electron with momentum $\mathbf{p}' = M\mathbf{p}$ on sublattice β in one layer hops to a momentum \mathbf{k} on sublattice α in the other layer.

In a pi -band tight-binding model the projection of the wavefunctions of the two layers onto a given sublattice are:

$$|\psi_{\mathbf{k}\alpha}^{(1)}\rangle = \frac{1}{\sqrt{N}} \sum_{\mathbf{R}} e^{i\mathbf{k}(\mathbf{R}+\tau_{\alpha})} |\mathbf{R} + \tau_{\alpha}\rangle \quad (2.16)$$

and

$$|\psi_{\mathbf{p}'\beta}^{(2)}\rangle = \frac{1}{\sqrt{N}} \sum_{\mathbf{R}'} e^{i\mathbf{p}'(\mathbf{R}'+\tau'_{\beta})} |\mathbf{R}' + \tau'_{\beta}\rangle \quad (2.17)$$

In our case, $\tau_{\alpha} = 0$, $\tau_{\beta} = \tau$, and \mathbf{R} is summed over the triangular Bravais lattice. Using the above equations and the two-center approximation, we get,

$$\langle \mathbf{R} + \tau_{\alpha} | H_T | \mathbf{R}' + \tau'_{\beta} \rangle = t(\mathbf{R} + \tau_{\alpha} - \mathbf{R}' - \tau'_{\beta}) \quad (2.18)$$

for the interlayer hopping amplitude in which t depends on the difference between the positions of the two carbon atoms. We find that

$$T_{\mathbf{k}\mathbf{p}'}^{\alpha\beta} = \sum_{\mathbf{G}_1\mathbf{G}_2} \frac{t_{\bar{\mathbf{k}}+\mathbf{G}_1}}{\Omega} e^{i[\mathbf{G}_1\tau_\alpha - \mathbf{G}_2(\tau_\beta - \tau) - \mathbf{G}'_2 \cdot \mathbf{d}]} \delta_{\bar{\mathbf{k}}+\mathbf{G}_1, \bar{\mathbf{p}}'+\mathbf{G}'_2} \quad (2.19)$$

where, Ω is the unit cell area, $t_{\mathbf{q}}$ is the Fourier transform of the tunneling amplitude $t(\mathbf{r})$, the vectors \mathbf{G}_1 and \mathbf{G}_2 are summed over reciprocal lattice vectors, and $\mathbf{G}'_2 = M\mathbf{G}_2$. Here, momentum is measured relative to the center of the Brillouin zone and not relative to the Dirac point.

The continuum model for H_T is obtained by measuring wave vectors in both layers relative to their Dirac points and assuming that the deviations are small compared to Brillouin-zone dimensions. Although t_q is not precisely known, it should fall to zero very rapidly with q on the reciprocal lattice vector scale. This is because the graphene layer separation exceeds the separation between carbon atoms in a layer by more than twice.

The largest t_q values that enter the tunneling near the Dirac point have $q = k_D$, the Brillouin-zone corner (Dirac) wave vector magnitude, and correspond to the three reciprocal vectors 0, $G^{(2)}$, and $G^{(3)}$ where the latter two vectors connect a Dirac point with its equivalent first Brillouin-zone counterparts (See fig. 2.6). When only these terms are retained, we get,

$$T^{\alpha\beta}(\mathbf{r}) = w \sum_{j=1}^3 \exp(-i\mathbf{q}_j \cdot \mathbf{r}) T_j^{\alpha\beta} \quad (2.20)$$

where $w = t_{k_D}/\Omega$ is the hopping energy,

$$T_1 = \begin{bmatrix} 1 & 1 \\ 1 & 1 \end{bmatrix} \quad T_2 = e^{-iG^{(2)\prime} \cdot \mathbf{d}} \begin{bmatrix} e^{-i\phi} & 1 \\ e^{i\phi} & e^{-i\phi} \end{bmatrix} \quad T_3 = e^{-iG^{(3)\prime} \cdot \mathbf{d}} \begin{bmatrix} e^{i\phi} & 1 \\ e^{-i\phi} & e^{i\phi} \end{bmatrix} \quad (2.21)$$

and $\phi = 2/3$. The three \mathbf{q}_j 's are Dirac model momentum transfers that correspond

to the three interlayer hopping processes. For $\mathbf{d} = 0$ and a vanishing twist angle the continuum tunneling matrix is $3w\delta_{\alpha A}\delta_{\beta B}$, independent of position.

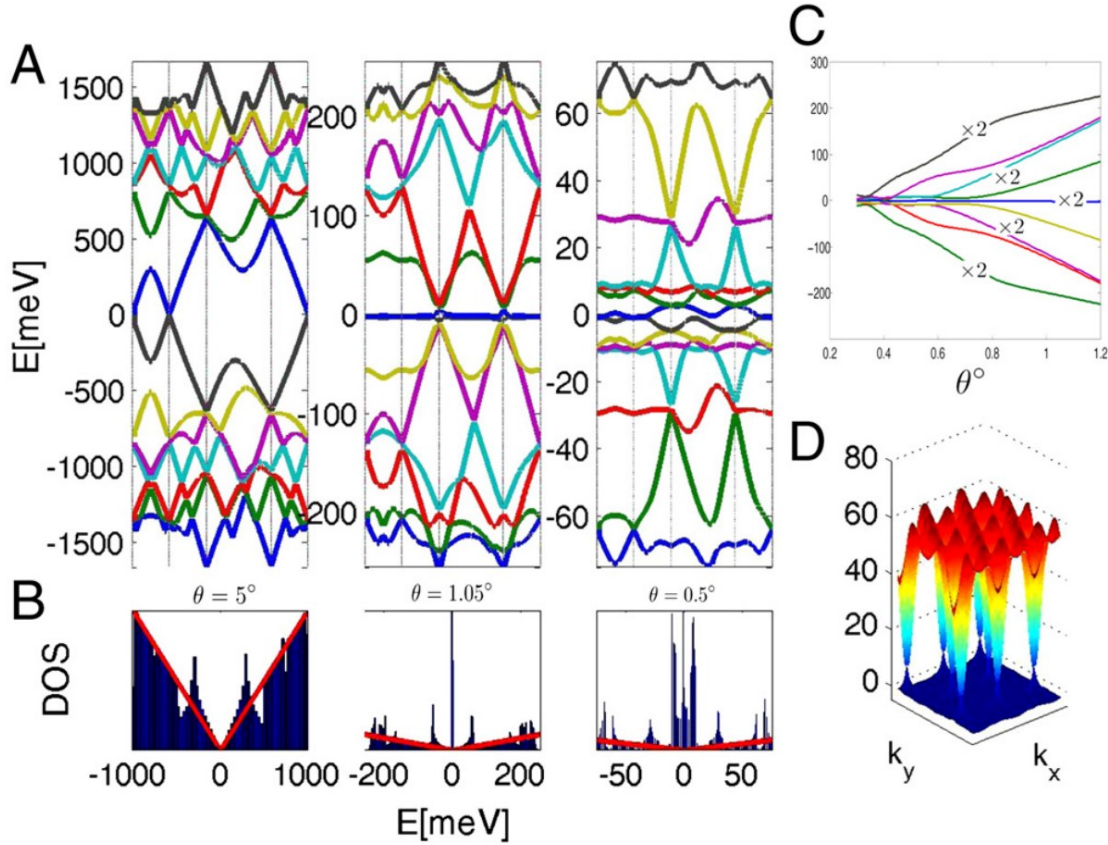


Figure 2.7: Cont. Figure adapted from [Bistritzer12233]

In the continuum model hopping is local and periodic, allowing Bloch's theorem to be applied at any rotation angle irrespective of whether or not the bilayer is crystalline. Solving the moiré bands numerically using the plane wave expansion illustrated in fig. , convergence is attained by truncating momentum space at lattice vectors of the order of $w/\hbar v$.

Up to a scale factor the moiré bands depend on a single parameter, $\alpha = w/vk_\theta$. Evaluating the moiré bands as a function of their Brillouin-zone momentum \mathbf{k} for different twist angles, we get results as shown in fig. . For large twist angles the low-energy spectrum is virtually identical to that of an isolated graphene sheet, except that the velocity is slightly renormalized. Large interlayer coupling effects appear only near the high energy van Hove singularities discussed by Andrei.

As the twist angle is reduced, the number of bands in a given energy window increases and the band at the Dirac point narrows. As illustrated in fig., we instead find that the Dirac-point velocity vanishes already at $\theta \approx 1.05^\circ$, and that the vanishing velocity is accompanied by a very flat moiré band which contributes a sharp peak to the Dirac-point density-of-states (DOS). At smaller twists the Dirac-point velocity has a nonmonotonic dependence on twist angle, vanishing repeatedly at the series of magic angles illustrated in fig. .

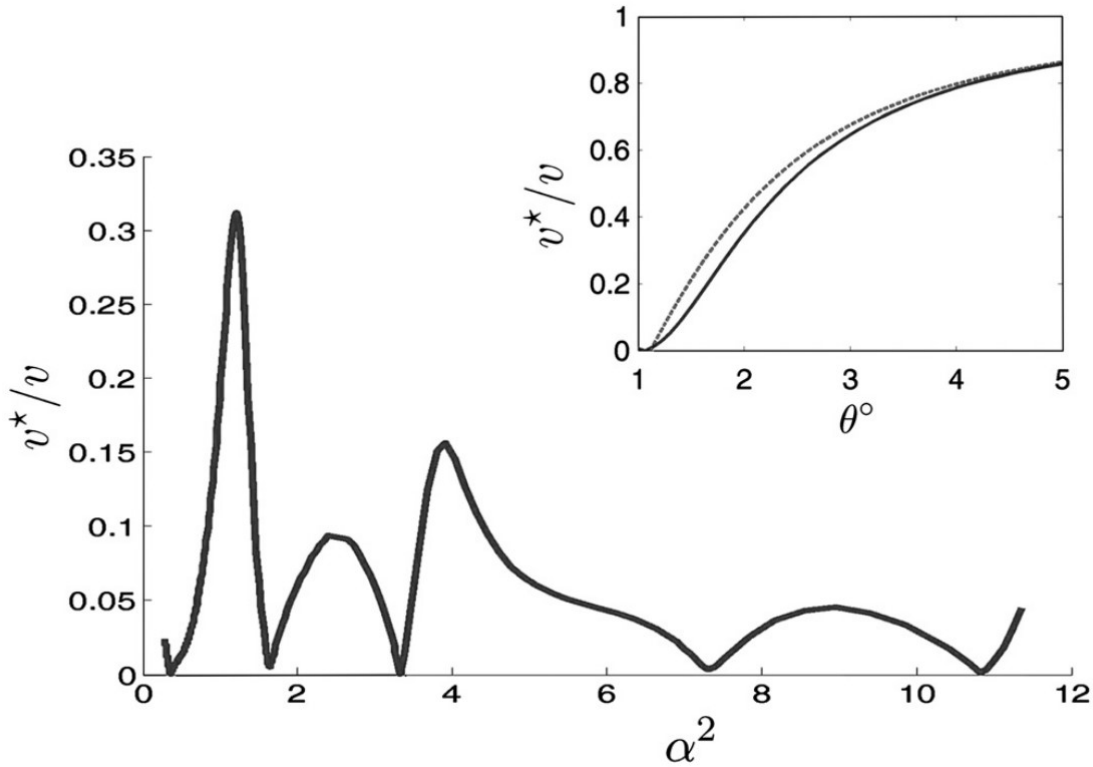


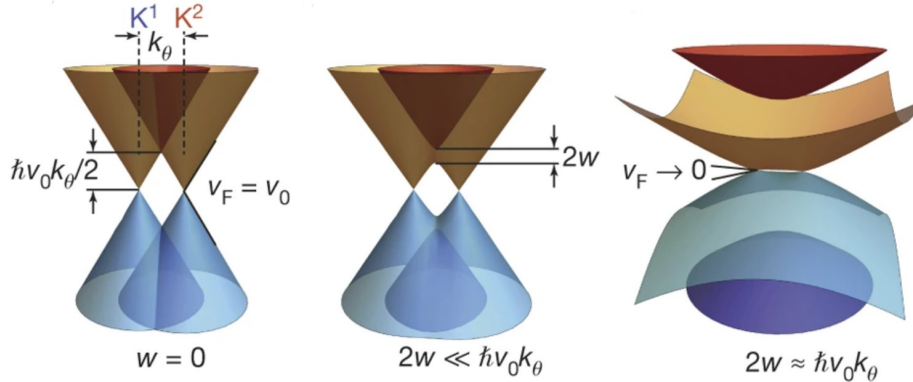
Figure 2.8: Cont. Figure adapted from [Bistritzer12233]

2.3.3 Flat bands in twBLG

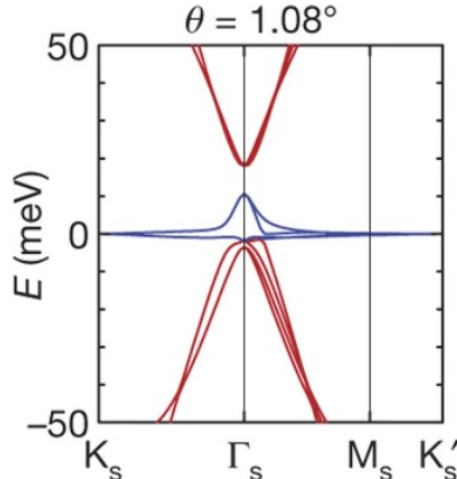
Two graphene layers twisted at an angle with respect to each other gives rise to the formation of a mini Brillouin zone. The twist angle θ displaces the individual monolayer Dirac points by a wave-vector $|k_\theta| = 2|K|\sin(\theta/2)$, hence forming the mini BZ.

There is hybridisation of the moiré bands leading to gap openings at the intersection of the Dirac cones and renormalisation of the Fermi velocity due to the

interlayer coupling between the two graaphene layers. A series of magic angles, $\theta = 1.05^\circ, 0.5^\circ, \dots$ have been found at which the Fermi velocity at the Dirac points vanishes that gives rise to flat moire bands with large density of states. The flat bands are formed as a result of competition between the interlayer hybridisation energy and the kinetic energy. When the hybridisation energy, $2w$, becomes comparable to the kinetic energy, $\hbar v_F k_\theta$, the lower hybridised states are moved to zero energy leading to bands with very narrow band width.



(a) Illustration of the effect of interlayer hybridization for $w = 0$, $2w \ll \hbar v_0 k_\theta$ and $2w \approx \hbar v_0 k_\theta$, where $v_0 = 10^6 \text{ ms}^{-1}$ is the Fermi velocity of graphene. Figure adapted from [Cao2018]



(b) The band energy E of magic-angle ($\theta = 1.08^\circ$) TBG calculated using tight-binding method. The bands shown in blue are the flat bands. Figure adapted from [Cao2018]

Figure 2.9: Electronic band structure of twBLG

2.3.4 Experimental Signatures of twBLG

The single particle picture breaks down, due to the presence of flat bands with large density of states near the charge neutrality point, because the Coulomb interactions exceed the kinetic energy in the system. twBLG enters various strongly correlated and topological states, when the Fermi energy is tuned within the flat bands. It has been experimentally observed to show correlated insulating states, superconductivity, quantum anomalous Hall effect and ferromagnetism.

Each moire superlattice band is four-fold degenerate at low twist angles. The charge density required to fill one superlattice band is given by:

$$n_s = \frac{4}{A} = \frac{8\theta^2}{\sqrt{3}a^2} \quad (2.22)$$

where A is the area of the moire unit cell. The filling factor, $v = 4n/n_s$ gives the number of electrons per moire unit cell. We see from the fig. 2.10 the presence of resistance peaks at full filling ($v = 4$), quarter ($v = 1$), half ($v = 2$) and three-quarter filling ($v = 3$). The insulating states at the full filling are due to the superlattice gap, i.e., it is a band insulator. But the insulating states at quarter, half and three-quarter filling are due to electronic correlations, hence termed correlated insulator. Near the correlated insulating states, the resistance goes to zero, showing the presence of superconducting states. The similarity of these superconducting states to the cuprates suggests a unconventional electronic origin to the superconductivity.

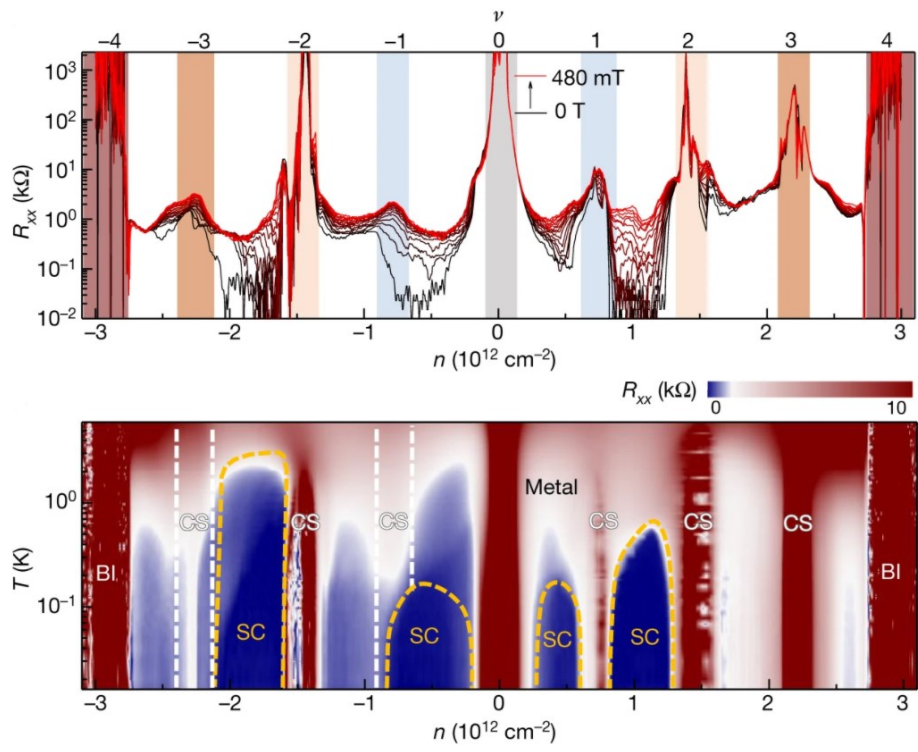


Figure 2.10: twBLG transport signatures. Top: Four-terminal longitudinal resistance plotted against carrier density at different perpendicular magnetic fields from 0 T (black trace) to 480 mT (red trace). Bottom: Colour plot of longitudinal resistance against carrier density and temperature, showing different phases including metal, band insulator (BI), correlated state (CS) and superconducting state (SC). Figure adapted from [Lu2019]

Chapter 3

Methods

In this chapter, we will discuss the experimental techniques that are used to fabricate twisted bilayer graphene devices. The fabrication of the devices is a very important step as many things in this step determine whether we will observe certain feature in our measurements. In this experiment, we need to have a twist angle between the graphene to be close to magic angle, i.e., 1.1° . The thickness of the tunnel barrier hBN and the alignment of the flakes are also important in the making of these devices.

3.1 Exfoliation of Graphene and hBN

There are various ways of preparing graphene flakes. [Bhuyan2016] The notable ones are Mechanical Exfoliation and Chemical Vapour Deposition (CVD). CVD can be used to grow large scale continuous graphene sheets in the order centimeters. But this method doesn't produce graphene flakes that have good electron mobility like in the case of Mechanical Exfoliation. We use Mechanical Exfoliation in our experiments.

In this method, we exfoliate graphene flakes onto Si-SiO₂ substrate. We have Si-SiO₂ substrate cut into small pieces of approximately 1.5cm*1.5cm. We then clean the wafers using sonication, in which the wafers are put in a beaker of acetone and sonicated in either normal or soft mode for 5mins. The wafers are then dipped in IPA and blow dried using N₂. These steps remove the organic adsorbates from the substrate surface. We worked with three variations of Mechanical Exfoliation:

- Conventional Exfoliation: We place a chunk of natural graphite on a Scotch tape

and subsequently cleave it to the fresh regions of the tape, uniformly distributing on the tape. This tape is called the Master Tape. The graphite crystals are then transferred from Master Tape onto a new tape by adhering the second tape to the first and slowly peeling it away. This process is repeated till thin translucent graphite crystals containing tape is made. This step ensures that we have flat regions of graphite on the tape surface. This tape is then stuck on the substrate and we gently apply pressure using a plastic dropper. We peel off the tape slowly. When the tape is removed, van der Waals force between the substrate and the top layers of the graphite crystals will pull down flakes of graphite ranging from 0.34nm (monolayer graphene) to hundreds of nanometers

- Hot Exfoliation: We follow the same steps as in conventional exfoliation, with one variation. We heat the substrate using a hot plate at $100^{\circ}C$ for 2-3 mins before sticking the tape onto it. This will improve the adhesion between graphite crystals and substrate.
- Oxygen Plasma Exfoliation: Here also we follow the same steps as in conventional exfoliation, with one variation. We clean the substrate using oxygen plasma cleaner before sticking the tape on it. This step helps in removing adsorbates from the surface of the substrate, hence improving the flake transfer, both in number and size.

We use Hot Exfoliation to get graphene flakes for our devices. The reason we don't use oxygen plasma is because the flakes obtained by this method are hard to pickup using dry transfer method (sec 3.3). We are looking for large monolayer graphene.

We use conventional Mechanical Exfoliation to get hexagonal Boron Nitride (hBN) flakes. The method is similar to that for graphene, with hBN crystals used instead of graphite while making the master tape. We use hBN crystals from Japan, that are known to give good quality thin flakes. We are looking for hBN with two different thicknesses - <5nm (thin hBN) and around 30nm (thick hBN). The thin hBN

is used as the tunneling barrier between twBLG and gold pads, while thick hBN is used as top and bottom hBN next to the gate.

3.2 Flake selection

3.3 Stamp creation

Stacks of graphene and hBN are created by putting them on top of each other, using Pickup and Transfer process. This process involves the use of polymer stamps that can stick to a flake and pick it up. The stamp consists of a coverslip with PPC or PC on hemispherical PDMS. The first step is to make the PDMS coverslips. The protocol is as follows:

1. Sonicate coverslips in acetone, wash with IPA and blowdry in N2.
2. Bake the coverslips for 5 minutes at 150 ° C to remove moisture.
3. Mix 10 parts PDMS with 1 part curing agent on a clean glass slide using a clean toothpick.
4. Put PDMS onto the coverslips by using a toothpick, picking up some PDMS mixture by holding the toothpick vertically.
5. Bake the coverslips at 150 ° C for 30 min.

A layer of PPC or PC is now added on PDMS that is used to pickup the flakes. The steps for this are:

1. Put a drop or two of PPC (15 percent PPC in anisole) or PC (6 percent PC in Chloroform) on PDMS coverslip using a dropper.
2. Spin coat it at 3000rpm for 30s, by attaching the coverslip to the spin coater with a double sided tape.
3. Keep the coverslip immediately on the hot plate to bake at 70°C for 10 mins.

PPC or PC solution has to be kept ready before starting stamp making. For making PPC solution:

1. Take a small glass bottle, wash it and heat it at $80^{\circ}C$ for 1hr 30min.
2. Measure and transfer 10ml of Anisole in the bottle and add 1.5g of PPC crystals in it, making a solution.
3. Shake the bottle vigorously and leave overnight.

For making PC solution:

1. Wash a small glass bottle.
2. Measure and transfer 3ml of Chloroform in the bottle and add 0.18g of PC crystals in it.
3. Leave the bottle overnight.

This coverslip is stick on the transfer stage using a metal stick. This is done with following steps:

1. Keep the coverslip on the metal stick and add EL-9 along the edges of the coverslip using a micro pipette.
2. Bake this at $90^{\circ}C$ on the hot plate for 2-3 mins.
3. Attach the metal stick to the stage using double sided tape.

3.4 Pickup and Transfer Process

Let's discuss the pickup and transfer process. After the PPC-PDMS and/or PC-PDMS stamp is ready, this process called the dry transfer technique [Kim16] [Wang614] is started in the transfer setup (shown in fig.). PC-PDMS stamp is used for thin hBN transfer and PC-PDMS stamp for everything else. The choice is based on the optimisation. The pickup and transfer protocol is as follows:

Part 1: Making a transfer boundary

1. Cover the microscope stage with Kaptan tape and put a little square of double sided tape on top of it.
2. Now a transfer boundary is made on PDMS. A piece of clean silicon wafer is stuck on the double sided tape and transfer stage metal stick is moved between the microscope stage and the objective.
3. Using the Piezo the coverslip is moved vertically till the PPC-PDMS or PC-PDMS is in focus and center the region with PDMS.
4. The PDMS is moved up and the empty wafer is brought into focus, and the stage heater temperature is set to $63^{\circ}C$ for PPC ($130^{\circ}C$ for PC).
5. The transfer stage is moved down slowly using the Piezo motors while keeping the wafer in focus. When the PDMS touches the wafer, a circle forms on the coverslip. The coverslip is held there for 5 seconds and then moved up. A circular boundary will be seen on the PDMS after this step. This is the transfer boundary where the PDMS will pick up flakes.
6. Finally, remove the wafer and the Kaptan tape.

Part 1 can be skipped once we are comfortable with the whole process.

Part 2: Pickup Step

1. Mount the wafer with the hBN/graphene flake to be picked in the same way as before, on the double double sided tape.
2. Follow similar steps as before, except now center the flake to be picked, directly under the transfer circle of PDMS.
3. Once the PDMS touches the wafer, go down till the circle spreads over the flake that needs to be picked.
4. Wait for 10 mins and turn off the heating.

5. Wait till the temperature comes down to around $35^{\circ}C$. Next, move the PDMS up and confirm if the flake got picked.
6. Finally, remove the wafer and the Kaptan tape.

Part 3: Transfer Step

Now there are two things that can be done. Either we keep on picking up flakes or transfer the flake/stack onto a clean wafer/gold pad. For the first case, we continue with the steps as above. We will have to take care of alignment during these steps. For the transfer, we perform the following steps:

1. Cover the microscope stage with Kaptan tape and put a little square of double sided tape on top of it.
2. Mount the wafer onto which the flake has to be transferred on the double sided tape and heat the stage to $75^{\circ}C$ for PPC ($180^{\circ}C$ for PC)
3. Touch the PDMS with the flake over the area to be transferred on and wait for 10 min.
4. Move the PDMS up and check if the flake got transferred.
5. Remove the wafer and the Kaptan tape.
6. Remove the coverslip from the transfer stick by dissolving EL-9 using acetone.
7. Finally, clean the coverslip and the wafer. They are kept in Anisole overnight (Chloroform for 2 hours) to dissolve the PPC (PC). Wash them with IPA (IPA and acetone), and blowdry with N_2 .

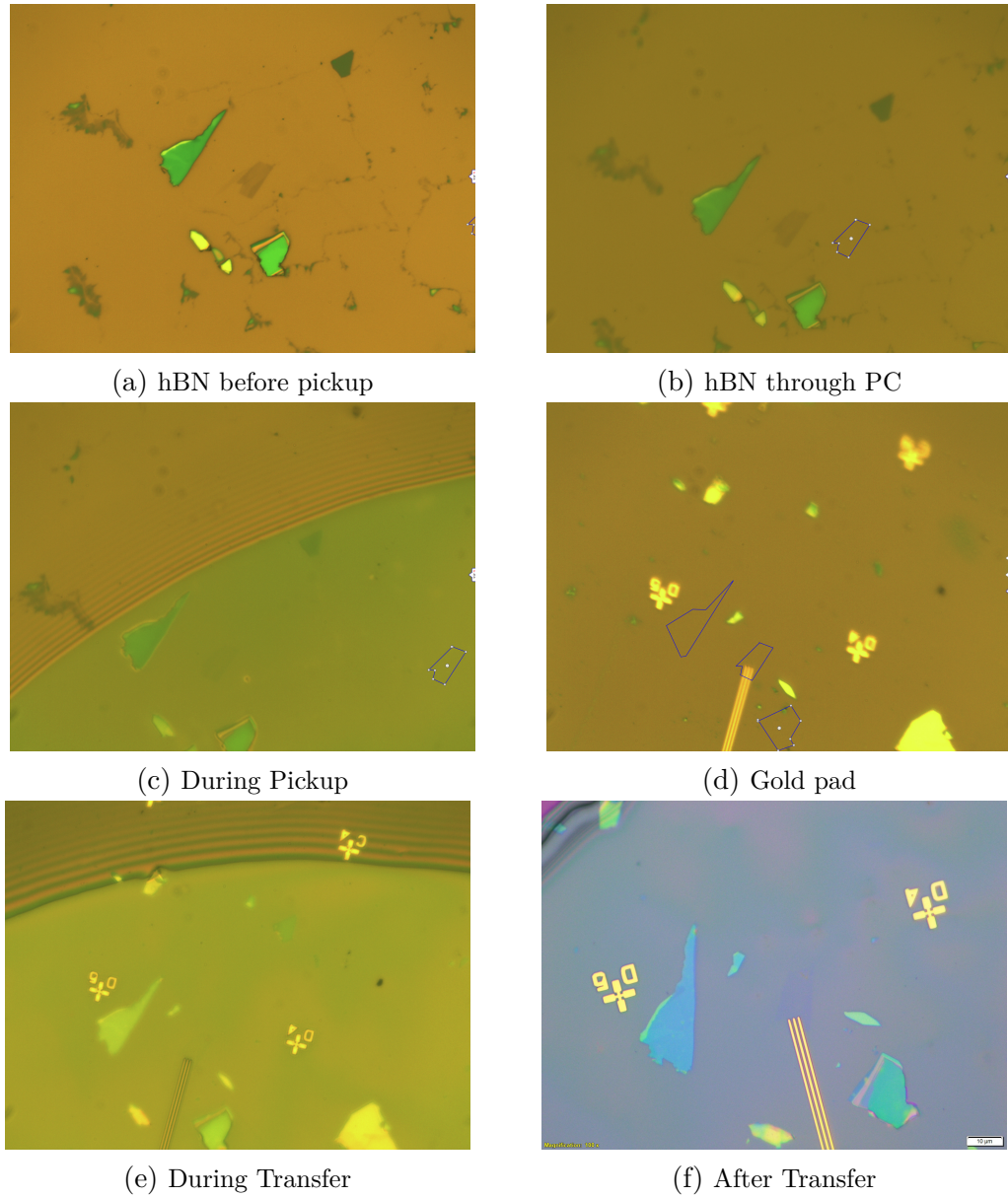


Figure 3.1: Pickup and Transfer of thin hBN on gold pad

3.5 Twisted Bilayer Graphene Fabrication

We need to make hBN-graphene-graphene-hBN-gold pad stacks for our devices. Here the top hBN encapsulates the twisted bilayer graphene. The two graphene flakes are aligned at magic angle of 1.1° . The hBN on the gold pad acts as a tunneling barrier. We have two parts in the whole process. One is to transfer thin hBN onto gold pad, the other is to make hBN-graphene-graphene stack on PPC. We follow the protocols as mentioned in sec 3.3, with one extra step during the stack preparation. We cut the

graphene using a tip and pickup one half of the flake with hBN, twist the stage at magic angle of 1.1° and pickup the other of the flake with graphene. We anneal the hBN-gold pad substrate, which helps in removing residues present on the flake, making it better for using it in our device. We then transfer the hBN-graphene-graphene stack onto the hBN-gold pad substrate, giving us the final stack. We can then proceed with drawing contacts.

Chapter 4

Measurements

Chapter 5

Conclusions

5.1 Discussion

5.2 Future Work